Journal of Magnetic Resonance 302 (2019) 72–87

Contents lists available at ScienceDirect

Journal of Magnetic Resonance

journal homepage: www.elsevier.com/locate/jmr

New experimental observations of the behavior of sodium ions in saturated rock samples

Evgeny Nimerovsky *

Department of Chemistry, New York University, New York, NY 10003, USA

ARTICLE INFO

Article history:
Received 7 February 2019
Revised 15 March 2019
Accepted 2 April 2019
Available online 3 April 2019

Keywords:
Static sodium NMR
Saturated rock samples
Diffusion regimes
Anisotropic motion
Bi-exponential relaxation
Lorentzian residual quadrupolar distribution

ABSTRACT

^{1}H NMR relaxometry of saturated rock samples has become a useful tool for the characterization of porosity and transport phenomena of enclosed fluids. The pore size can be measured using the difference between inverse relaxation values of protons absorbed by the saturated rock and that present in the bulk fluids. These experiments are usually performed at low magnetic fields to reduce the influence of the diffusion on the relaxation values in the presence of Internal Gradient Fields. Recently, sodium ions have become objects of investigation. The main advantage of sodium ions over protons as measured spins in the Petrophysic NMR experiments is their presence in water and not other phases like oil and gas. However unlike protons, sodium ions can have slow motion properties like appearance of the bi-exponential relaxation and residual quadrupolar distribution, which can lead to complex behavior of spins inside the pores. Here, we describe eight ^{23}Na NMR experiments at 9.39 T external magnetic field, in which we have investigated the behavior of sodium ions in 4 saturated rock samples: Berea 500, Fontainebleau 1, Bentheimer sandstones, and Austin chalk. We show that the reduction of spin-spin relaxation is caused by anisotropic motion and not diffusion in the presence of Internal Gradient Fields. There can be a link between free diffusional and motional averaging regimes regardless of the size of environment in which the measured spin ions are. Using different NMR sequences, we reveal and quantitatively describe bi-exponentially relaxing spins and spins with residual quadrupolar coupling. This work demonstrates unique model for the behavior of ions inside porous media, which is different than known models (Brownstein-Tarr model and "agarose gel model").

1. Introduction

Nuclear Magnetic Resonance (NMR) spectroscopy is widely used for the investigation of the behavior of the liquid and gas molecules within pore systems [1]. Pore size distributions [2–4] have been determined via relaxation time measurements in oil/gas reservoirs [5–8], biological tissue microstructures [9], and silica gels [10,11]. Measurements have been performed at low [5,12–14] and strong external magnetic fields [15–17] with both proton and sodium nuclei in brine [16,18–21]. When the influence of the diffusion [22] in the presence of Internal Gradient Fields [23] (IGFs) can be neglected, the link between the relaxation time of proton spins and the pore size is established via [24,25]:

$$T_i^{-1} = T_{i,bulk}^{-1} + \rho_i(S/V) \quad (1)$$

where $T_{i,bulk}$ is the spin-lattice ($i = 1$) or spin-spin ($i = 2$) relaxation time of the spins in bulk fluids (solution where the influence of the walls can be neglected and magnetic gradient fields are not induced), ρ_i is the surface relaxivity, and S/V is the surface-to-volume ratio of the pore. Additional inhomogeneity of the external field could be taken into account here as well.

The origin of IGFs is the susceptibility difference at the solid-liquid boundary [26], which can further be enhanced by the presence of paramagnetic impurities [27]. When the influence of diffusion in the presence of IGFs cannot be neglected (usually in strong external magnetic fields), Eq. (1) contains an additional diffusion term [15,28–30] T_D^{-1} for spin-spin relaxation:

$$T_2^{-1} = T_{2,bulk}^{-1} + \rho_2(S/V) + T_D^{-1} \quad (2)$$

Using the parameters of the diffusion length l_D, the distance traveled during a characteristic experimental delay time τ, the pore size l_S, and the dephasing length l_g, which is the distance of travel in order for a spin to dephase by 2π radians under the influence of IGFs, three main regimes can be distinguished, which in turn can be used to classify the measurement outcomes [27,31]:

* Current address: A127A Chemical and Life Sciences Lab, 600 South Mathews Avenue, University of Illinois at Urbana-Champaign, IL 61801, USA.
E-mail address: en5@illinois.edu

https://doi.org/10.1016/j.jmr.2019.04.002
1090-7807/

(1) When $l_D \ll l_S, l_g$, the measured spins are in the free diffusional regime. In this case, the diffusion term T_D^{-1} is proportional to τ^2.
(2) When $l_S \ll l_D, l_g$, the spins are in the motional averaging regime[31]. In this case, they experience a motionally averaged IGFs, and the diffusion term T_D^{-1} does not depend on τ, and is inversely proportional to the diffusion coefficient.
(3) When $l_g \ll l_D, l_S$, the measured spins are in the so-called localization regime [31]. T_D^{-1} does not depend on τ and is proportional to the cubic root of the diffusion coefficient. The signals of spins located within l_g of the wall are accentuated [15] because of their restriction in the motion near the walls. The measured signal in this regime is significantly smaller as compared to the one due to the other two regimes.

Multi-exponential proton T_2 values were previously observed with CPMG at strong external magnetic fields (9.39 T) and mono-exponential values at low magnetic fields (0.3 T) (Ref. [15], Fig. 6). It was suggested that this behavior may be due to the spins being in the 'pre-asymptotic localization regime', and that multiple gradient oscillations may be traversed by the spins. Therefore, the study of saturated rock samples is thought to be challenging at strong external magnetic fields, and is generally avoided.

The advantage of using ^{23}Na as the measured spin, especially in the context of Petrophysics, is that, only water contains sodium, whereas proton is found in other phases as well [16] (oil and gas). However, the ionic property of sodium in the brine presents some extra complexity. Additionally, ^{23}Na has a quadrupolar moment [32], which reduces the relaxation times and the appearance of fast and slow motion regimes (these regimes are not linked to the diffusion).

In the case of the slow motion regime, where the motion is limited, sodium can exhibit bi-exponential relaxation because of slow exchange, which leads to the appearance of two T_1 and two T_2 time constants [33,34]. These values are defined by spectral densities J_0, J_1, J_2 (Ref. [35]) as shown below:

$$T_{1f} = 2J_1, T_{1l} = 2J_2; T_{2f} = J_0 + J_1, T_{2l} = J_1 + J_2 \quad (3)$$

The actual values of $J_m (m = 0 - 2)$ are defined in different ways, depending on convention [34–36]. For example, the spectral densities can be defined as in the Ref. [35]:

$$J_m(m\omega_0) = \frac{(2\pi)^2}{20} \frac{\chi^2 \tau_c}{1 + (m\omega_0 \tau_c)^2} \quad (4)$$

where τ_c is the correlation time, ω_0 is the Larmor frequency and χ is a root-mean-square quadrupolar coupling constant.

In the case of the fast motion regime or motional narrowing, the spectral densities are equal:

$$J_0 = J_1 = J_2 = \frac{(2\pi)^2}{20} \chi^2 \tau_c \quad (5)$$

which also results in the equality of relaxation times ($T_2 \cong T_1$).

There is also the possibility that sodium ions display a residual quadrupolar distribution, especially in the presence of electric field gradients [37,38].

As mentioned previously [20,21], interpretation of the change of the relaxation times or appearance of the multi-exponential decay of sodium ions inside porous media could not be explained in the same way as in the case of protons, using the Brownstein-Tarr model [39]. However, as shown in this article it also cannot be explained by the another model where bi-exponential relaxation is only assumed, for e.g. sodium ions in agarose gel [40]. Such model can be named as "agarose gel model", which was used for investigations of sodium ions relaxations in mesoporous systems [20] and Stevns Klint chalk [21].

Herein, we present experimental measurements of sodium ions in rock samples saturated with brine at an external magnetic field (9.39 T). The samples include Berea 500, Fontainebleau 1, Bentheimer sandstones, and Austin chalk. By processing different NMR experimental data we reveal unique behavior of sodium ions inside porous media, which cannot be explained with the known models. The observations include – (1) completely different influence of the pore surface on the relaxation rates of sodium ions with respect to protons and sodium ions in agarose gel, (2) transfer of free diffusional regime into motional averaging regime, and (3) different populations of sodium ions with bi-exponential relaxation and residual quadrupolar distribution. The second observation, (2), can be detected in the bulk fluids, too. We demonstrate this with two different consentrations of LiCl solution in 5 mm tubes.

2. Experimental methods

2.1. NMR sequences:

Fig. 1 shows 8 experimental pulse sequences, which were used in our investigation.

The experimental pulse sequences (Fig. 1a–f) are well known and are widely used in NMR experiments, whereas the last two sequences (Fig. 1g,h) are new. The goals of using the Triple Quantum Filter (TQF) methods [35] (Fig. 1e,f) and Quadrupolar Sensitive Pulse (QSP) [44] methods (Fig. 1g,h) are to assess the presence of bi-exponentially relaxing spins and spins with residual quadrupolar coupling.

QSP method (Fig. 1g) is sensitive to the slow motion regime, and does not excite fast motion regime (under the condition that the inhomogeneity of the external field is small with respect to radio-frequency field, ν_{rf}), as described previously. QSP pulse consists of 2 pairs of adjacent pulses with alternative phases and 180°-pulse between them. The lengths of these four pulses are the same and equal to: $t_{p,\kappa} = (4\nu_{rf}\kappa)^{-1}$, where $\kappa \geq 1.25$. QSP experiment can be used for measurement of the quadrupolar coupling via comparison of the experimental QSP curves (central transition intensities as function of κ) with simulated, as was proposed in Ref. [44].

The last method (Fig. 1h) is a modified Spin Echo experiment, where the first 90°-pulse is replaced by the QSP-pulse. In this case, the durations of the pulses around the 180°-pulse ($t_{p,\kappa}$) in QSP-pulse are chosen such that a signal of sodium ions with quadrupolar coupling appears at maximum intensity. This requires optimization of two parameters - ν_{rf} and κ.

2.2. Calculations and simulations

Simulations of the pulse sequences (SE, longitudinal and transverse TQFs, QSP and QSP-SE) were performed using MATLAB software, the MathWork Inc.. The numerical simulations were performed using a set of tensor differential equations as described in Ref. [35]. In order to take into account the influences of the bi-exponential relaxation and residual quadrupolar interaction during the acquisition time, which are present in the NMR experiments, the simulations were performed with 80 us of dwell time and 40 ms of acquisition time and the simulated signals were transformed into frequency domain.

The Inversion Laplace Transform (ILT) of the IR, CPMG and SE experiments were done using the algorithm described in Ref. [45], where the imposed regularity control parameter (α) was chosen as 0.2. 350 number of bins were used in relaxation time grid. The space was logarithmic in range of [0.03:316] (ms).

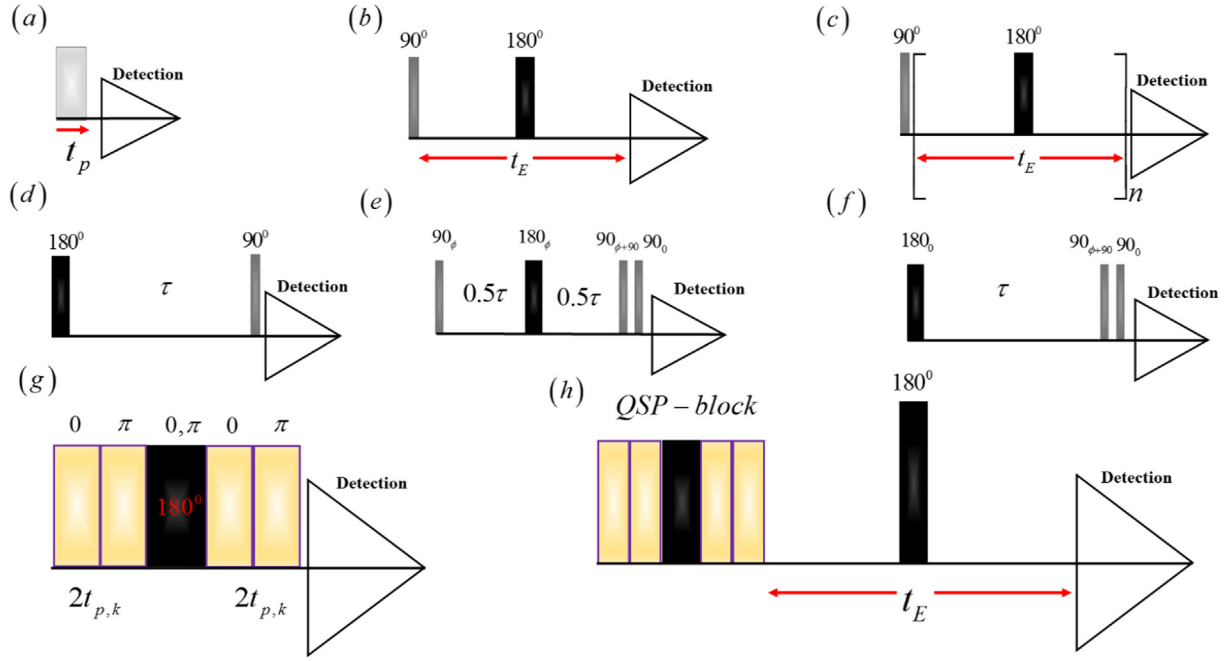

Fig. 1. (a) Single Pulse (SP) experiment, where the flip angle of the exciting pulse is a variable; (b) Spin Echo (SE) method [41], where the delay time t_E is a variable; (c) Carr-Purcell-Meiboom-Gill (CPMG) method [42], where nt_E is a variable; (d) Inversion Recovery (IR) method [43], where the delay time τ is a variable; (e) Transverse Triple Quantum Filter (TQF) method [35], where the delay time τ is a variable; (f) Longitudinal Triple Quantum Filter (TQF) method [35], where the delay time τ is a variable; (g) Quadrupolar Sensitive Pulse [44] (QSP), where the flip angles of the four pulses, except 180°-pulse in the middle, are variables: $t_{p,\kappa} = (4\nu_{rf}\kappa)^{-1}$, $\kappa \geq 1.25$ and ν_{rf} is the radio-frequency field of the pulses; (h) Modified QSP-SE method, where instead of 90°-pulse QSP-pulse is used and the delay time t_E is a variable.

Linear fitting including mono- and bi-exponential were performed using the Levenberg-Marquardt algorithm.

2.3. Materials

Four saturated rock samples, a Berea 500 sandstone, a Fontainebleau 1 sandstone, a Bentheimer sandstone, and an Austin chalk were acquired from Schlumberger-Doll Research, Cambridge, USA. Each rock sample was cleaned and cut into a cylindrical plug with a 22.35 mm diameter and 42.21 mm of height. The samples were saturated with 0.55 M of NaCl solution (32 ppk) for over 48 h to reach full equilibrium [16]. Before each experiment, the rock sample was taken out of the brine and wrapped with Parafilm (Pechiney Plastic Packaging Company, Chicago, IL) to prevent fluid loss.

Previously it was shown that all three sandstones have a macroscopic single-modal distribution of the pore system [6,7,15,46,47], where on average the size of pores in Berea 500 was around 15–20 μm, 20–50 μm in the case of Fontainebleau 1, and 30 μm in the case of Bentheimer. Austin chalk has a dual microscopic pore system [48], where the size ranges between 5 and 7 μm.

The sample with standard PBS solution (0.137 M of NaCl) was packed into a plastic tube with a diameter of 18 mm.

Two samples with 0.5 M and 15 M of LiCl solutions were packed into glass tubes with a diameter of 5 mm.

2.4. NMR experiments

All experiments were performed using a broad-brand direct observe probes tuned to sodium in the case of ^{23}Na experiments and lithium in the case of ^{7}Li experiments on a Bruker Avance, 400 MHz spectrometer. Bruker MICWB40 probes were used to collect the data, with a dual-tuned, 25 mm i.d. ^{1}H/^{23}Na and ^{1}H/^{7}Li coil inserts. Nutation frequencies for ^{23}Na NMR were calibrated using a 5 mm quartz tube with 0.4 M solution of NaCl. In the case of ^{7}Li, the same samples were used for nutation frequency calibration.

Tables 1–3 list the experimental parameters used.

3. Results and discussions

Fig. 2 shows the single pulse ^{23}Na spectra in the four different rock samples (Berea 500, Fontainebleau 1, Bentheimer and Austin) after 90°-pulse excitation, using highest available ν_{rf} for this probe (4 kHz).

Berea 500 (Fig. 2, pink line) has the least intense but broadest peak and the largest offset with respect to NaCl solution. The width of almost 16.25 ppm for Berea 500 exceeds broadening that one could expect from inhomogeneities due to diamagnetic susceptibility alone, and quadrupolar broadening or broadening due to paramagnetic impurities may be expected. Berea 500 is known to exhibit strong IGFs (Ref. [27]), which are perceptible even at low magnetic field [49]. The ratios of the peak integrals of Bentheimer:Austin:Berea 500:Fontainebleau 1 are 1:0.87:0.66:0.53.

3.1. Transverse TQF experiments

The potential influence of a quadrupolar interaction and associated quadrupolar relaxation needs to be investigated as well,

Table 1
Experimental parameters used in SP, SE, CPMG, IR experiments (Fig. 1a–d).

Materials	NS[a]	SW[b] (kHz)	AQ[c] (s)	D1[d] (s)
LiCl:0.5 M/15 M	1/1	8/8	0.51/0.51	200/100
NaCl	40	25	0.1	0.25
Rocks	96	25	0.05	0.25

[a] Number of Scans.
[b] Spectral Width.
[c] Acquisition time.
[d] Recycle delay.

Table 2
Experimental parameters used in TQFs experiments (Fig. 1e and f).

Materials	Methods	NS[a]	SW[b] (kHz)	AQ[c] (s)	D1[d] (s)
Sandstones	Trans_TQF	3600	25	0.05	0.4
Austin	Trans_TQF	480	25	0.05	0.4
	Long_TQF	2400	25	0.05	0.4

[a] Number of Scans.
[b] Spectral Width.
[c] Acquisition time.
[d] Recycle delay.

Table 3
Experimental parameters used in QSP and QSP-SE experiments (Fig. 1g-h).

Materials	Methods	NS[a]	SW[b] (kHz)	AQ[c] (s)	D1[d] (s)
Austin	QSP	480	25	0.05	0.25
	QSP-SE	512	25	0.05	0.25

[a] Number of Scans.
[b] Spectral Width.
[c] Acquisition time.
[d] Recycle delay.

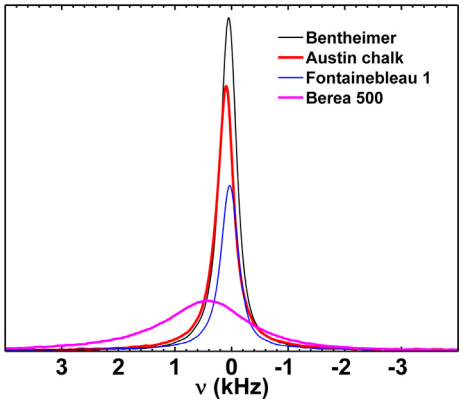

Fig. 2. ^{23}Na spectra of brine-saturated (32 ppk, ppk defined as g NaCl/kg H2O) in Bentheimer (black line), Austin (red line), Fontainebleau 1 (blue line) and Berea 500 (pink line). The resonance offsets of the peaks were calculated with respect to a NaCl solution (in the plastic tube) (0.135 M) and the full width at half height ($\Delta\nu$) was determined. In all cases, ν_{rf} = 4 kHz. Bentheimer: offset = 49 Hz, $\Delta\nu$ = 345 Hz; Austin chalk: offset = 89 Hz, $\Delta\nu$ = 350 Hz; Fontainebleau 1: offset = 34 Hz, $\Delta\nu$ = 364 Hz; Berea 500: offset = 450 Hz, $\Delta\nu$ = 1720 Hz. (For interpretation of the references to colour in this figure legend, the reader is referred to the web version of this article.)

which can be done with Multiple Quantum Filter methods [35]. Fig. 3 shows Transverse TQF (pulse sequence in Fig. 1e) spectra of sodium ions in four rock samples at different values of the delay time τ. 3600 scans and 480 scans were used for the sandstones and the Austin chalk, respectively. While there are some weak signals for the sandstones, only Austin chalk shows significantly intense signal (Fig. 3d, 2.3% with respect to 90° pulse excitation).

For Berea 500 (Fig. 3a) and Fontainebleau 1 (Fig. 3b), TQF signals are difficult to distinguish from noise. The sodium TQF signal in the case of Bentheimer (Fig. 3c) is the largest among the sandstones. Since all three sandstones contain IGFs, there is some loss of TQF intensity because of partial cancellation of anti-phase signals [50]. There is therefore a limit to the ability to quantify the amounts of bi-exponentially relaxing spins or spins with residual quadrupolar distribution.

Nonetheless, from these experiments, one may conclude that in the case of sandstones mono-exponentially relaxing sodium ions account for the major part of the visible signal, being in fast motion regime. Slow motion sodium ions represent a minor part. The possible source of the slow motion signal can be the spins involved in slow exchange between the surface and the bulk volume of the pores.

In the case of Austin chalk slow motion sodium ions are detected, which can have bi-exponential relaxation or residual quadrupolar distribution, since $T_3^{\pm1}$ operators are excited under both interactions [35].

3.2. Inversion recovery experiments

Fig. 4 shows the T_1 distribution obtained IR data using an ILT for the different rock samples.

As seen in Fig. 4, the T_1 distribution of sodium ions can be considered to be mostly mono-exponential, except for Austin chalk (Fig. 4e), where a significantly broader distribution is seen. All peaks for the NaCl solution (Fig. 4a) and the three sandstones (Fig. 4b–d) have almost the same width, whereas the width of the peak in the case of Austin chalk is 2.5 times larger. This feature could be seen as an indication that the distribution of the pore sizes is broader for Austin chalk than it is for sandstones. Sodium spins in Fontainebleau 1 (Fig. 4c, T1 = 53 ms), and Bentheimer (Fig. 4d, T1 = 52.35 ms) exhibit similar T_1 as a 0.135 M NaCl solution (T_1 = 53 ms). For Berea 500 (Fig. 4b), T_1 = 47.5 ms, which is only slightly shorter (10%). T_1 of ^{23}Na in Austin chalk (Fig. 4e) has the largest deviation, T_1 = 41 ms (23%). For sandstones, we can conclude that T_1 relaxation values of sodium ions are not influenced by the pore surface, whereas in the case of Austin chalk, there is an influence on T_1.

Taking into account TQF experimental results (Fig. 3), T_1 distributions (Fig. 4) and the known pore distributions of the investigated rock samples (single pore for sandstones and dual pore size distributions for Austin chalk), T_2 experiments should be done to demonstrate mono-exponential dependence of the measured signals for 3 sandstones and multi-exponential dependence for Austin chalk.

3.3. Qualitative comparison of CPMG and SE signals

For measurements of T_2 relaxation values, we performed CPMG and SE experiments under different experimental conditions of ν_{rf}

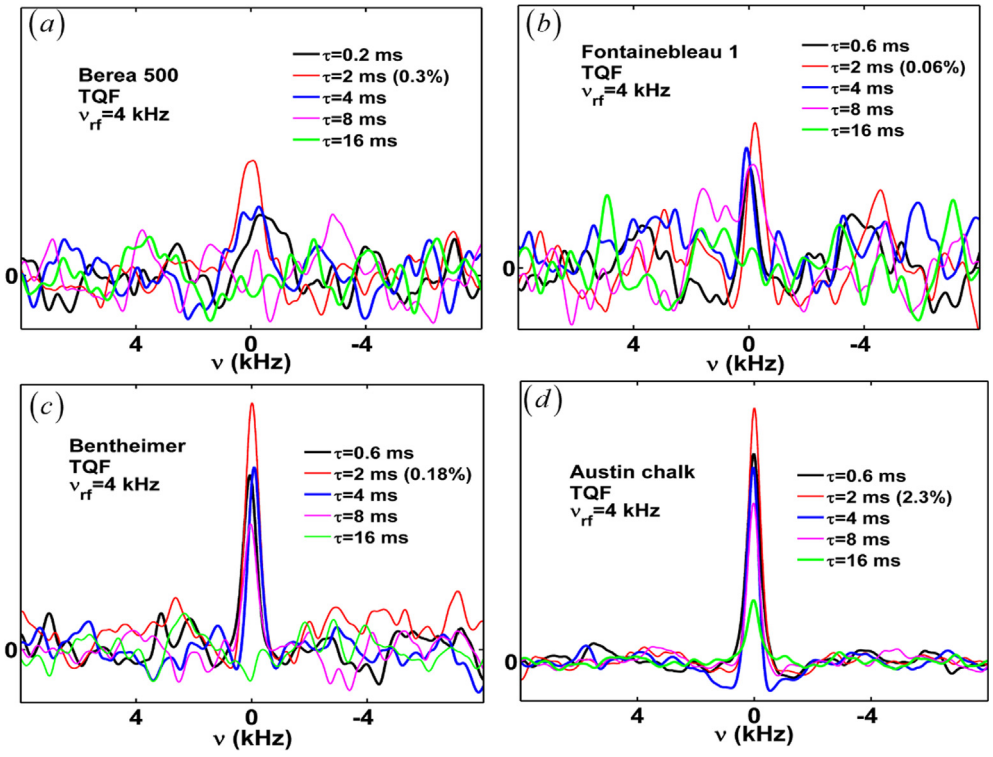

Fig. 3. ^{23}Na TQF spectra for different delay times τ for Berea 500 (a), Fontainebleau 1 (b), Bentheimer (c) and Austin chalk (d). τ: 0. 6 ms – black line (in the case of (a) it is 0.2 ms); 2 ms – red line; 4 ms – blue line; 8 ms – pink line and 16 ms – green line. The relative intensity of the red peak was calibrated with respect to 90°-pulse excitation. 3600 scans and 480 scans were used for the sandstones (a–c) and the Austin chalk (d) respectively. (For interpretation of the references to colour in this figure legend, the reader is referred to the web version of this article.)

and t_E. Figs. 5 and 6 show CPMG and SE experimental signals as function of time, respectively.

Comparing Fig. 5 with Fig. 6 a conclusion can be made that the CPMG signals decay significantly slower than SE signals. For example, for Berea 500, CPMG signals decay between $nt_E \in (0:65]$ ms (Fig. 5a), whereas SE signals decay between $t_E \in (0:20]$ ms (Fig. 6a). The same behavior can be found by comparing CPMG signals with SE signals of the other three rock samples.

ILTs of CPMG signals show multi-exponential distributions (Fig. A1b–e in Appendix A) for all four rock samples. ILTs of SE signals show mono-exponential distributions for sandstones (Fig. A2b–d in Appendix A) and multi-exponential for Austin chalk (Fig. A2e in Appendix A).

Taking into account TQF experimental data and knowledge about single pore distributions in the case of sandstones, the measured signals should have mono-exponential decay. Therefore, SE experimental data are more reliable with respect to CPMG experimental data.

The deviations of CPMG experimental data with respect to SE can be explained by the fact that some part of the macroscopic magnetization is not excited and converted properly during the range of pulses, especially with weaker rf-field due to the influence of IGFs.

For example, under conditions of t_E = 2.29 ms (Fig. 5a, blue line with squares), CPMG signal decays slower with respect to the case when t_E = 0.34 ms (Fig. 5a, red line with stars). For Fontainebleau 1 (Fig. 5b), a small change of t_E from 1.53 ms (red line with stars) to 1.55 ms (blue line with squares) has influence on the behavior of CPMG signal at longer times (greater than 20 ms). The same behavior can be found in for Bentheimer (Fig. 5c), where CPMG signals under different t_E values begin to diverge with respect to each other from 50 ms of nt_E.

SE signals in 3 cases (except Berea 500, Fig. 6a) also have a dependence on the experimental conditions. However, this dependence can be explained by the influence of the diffusion in the presence of IGFs for Fontainebleau 1 (Fig. 6b) and Bentheimer (Fig. 6c); and bi-exponential relaxation or residual quadrupolar interaction in the case of Austin chalk (Fig. 6d).

3.4. Quantitative processing of SE signals

Fig. 7 shows experimental SE signals under 4 kHz of rf-field and comparisons with single exponential decay signals. We fitted single exponential decay signals to Berea 500 (T_2 = 6.95 ms), Fontainebleau 1 (T_2 = 15.1 ms), and Bentheimer (T_2 = 17.7 ms), and a bi-exponential decay signal to the Austin data (T_2 = 1.6 and 11.3 ms with probabilities 0.32 and 0.68, respectively). For Berea 500 (Fig. 7a) and Austin chalk (Fig. 7d), the exponential decay signals fit the data well. For Fontainebleau 1 (Fig. 7b) and Bentheimer (Fig. 7c) these single exponential decay signals generally fit the data well, except for $t_E \geq 10$ ms.

It is clear that bi-exponential models (“agarose gel model”) also would not be suitable to describe the data for Fig. 7b,c. In the case of bi-exponential dependence of the signal, the signal decays faster at short times and slower at long times. If the measured signals in Fig. 7b,c would have bi-exponential dependence, the single exponential decay signals had to decay faster with respect to measured signals at long times. Fig. 7b,c show opposite behavior. Therefore the measured signals cannot be fit with bi-exponential decay signals.

This deviation can be explained by the influence of the diffusion, which in turn, can be assessed quantitatively (Fig. 8) assuming that the value of the effective T_2 changes with the delay time t_E.

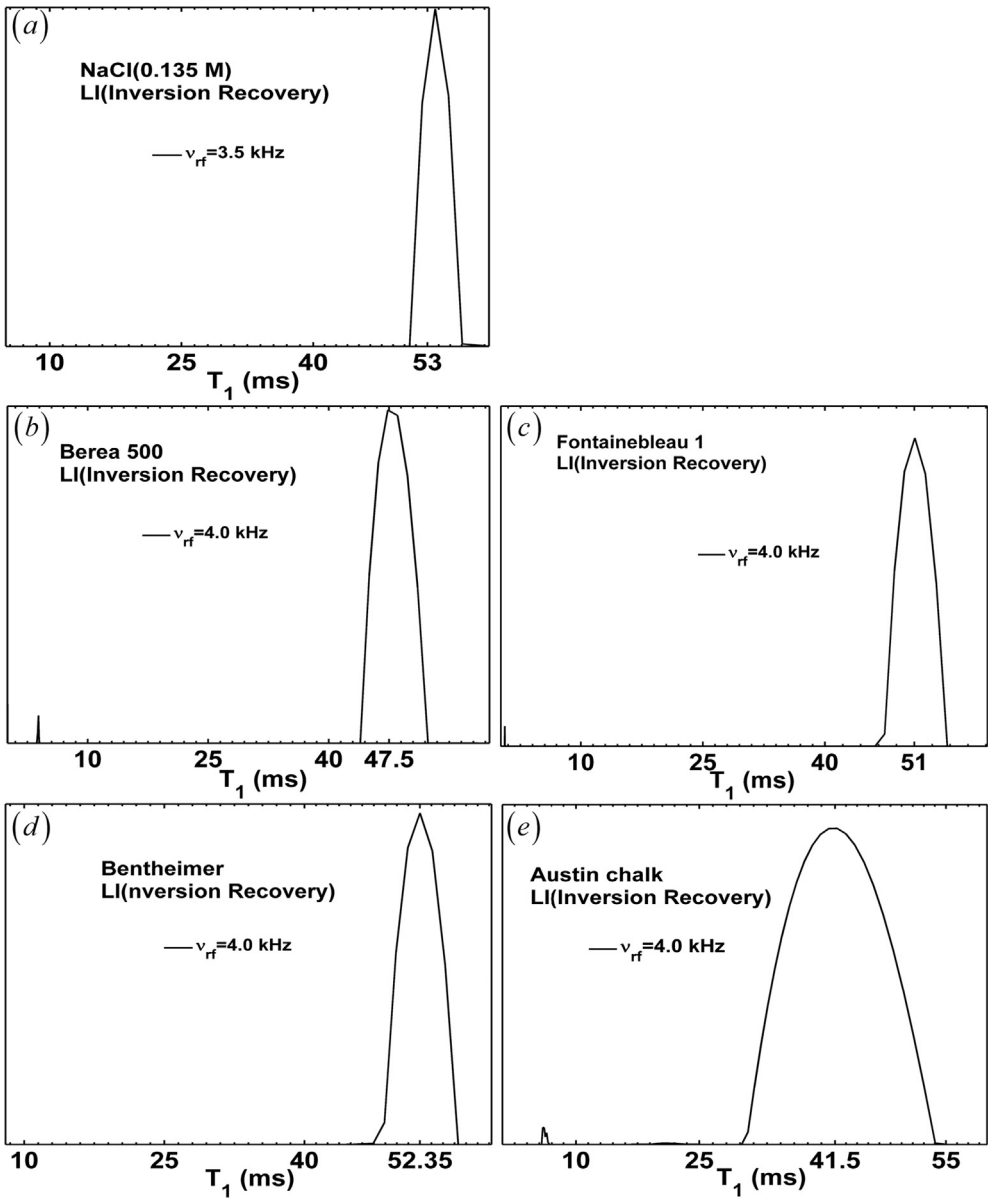

Fig. 4. T_1 probability distributions from ^{23}Na IR experiments in NaCl, which represents bulk sample (a), Berea 500 (b), Fontainebleau 1 (c), Bentheimer (d) sandstones and Austin chalk (e) under $\nu_{rf} = 3.5$ kHz in the case of (a) and $\nu_{rf} = 4$ kHz in other cases. The scale of the x-axis is linear.

Eq. (6) shows the dependence of inverse effective spin-spin relaxation on echo time:

$$T_{2,\mathrm{eff}}^{-1}(t_E) = T_2^{-1} + T_D^{-1}\left[1 - \exp\left\{-(t_E/B)^2\right\}\right] \tag{6}$$

With this formulation, the data for Fontainebleau 1 and Bentheimer fit quite well (Fig. 8).

The values of T_D and B of ^{23}Na in Fontainebleau 1 and Bentheimer are almost equal: $T_D = 52.08$ ms, $B = 28.6$ ms and $T_D = 69.4$ ms, $B = 29.4$ ms, respectively.

The time-dependence of $T_{2,\mathrm{eff}}^{-1}$ (Eq. (6)) proves an influence of the diffusion in the presence of IGFs, since effective spin-spin relaxation is decreased with increasing t_E.

Eq. (6) does not have a theoretical basis and was obtained experimentally. However, some conjectures can be made, taking into account possible regimes like free diffusional and motional averaging. In order to interpret the relationship between the parameters and these possible regimes, it is helpful to expand Eq. (6) into a Maclaurin series,

$$T_{2,\mathrm{eff}}^{-1}(t_E) \approx T_2^{-1} + \left(T_D B^2\right)^{-1} t_E^2 + \left(3T_D B^4\right)^{-1} t_E^4 + \cdots \tag{7}$$

It is clearly seen that if we take into account the first two terms of Eq. (7) (the constant and the t_E^2 term), this expression corresponds to the expression as in free diffusional regime [27]. At times $t_E > 1.7B$, the inverse of the spin-spin relaxation time (Eq. (6)) becomes time-independent like for motional averaging regime [27].

The parameter B defines how fast the inverse of the spin-spin relaxation achieves its plateau value. In the case where the brine is diluted, it should depend on the pore size l_S and inversely on the diffusion coefficient D_0, and hence may have a proportionality according to

$$B \propto l_S^2 / D_0 \tag{8}$$

Such inverse dependence of parameter B on D_0 and independence from IGFs can be simply explained by the fact that in the case of $D_0 \to 0$, IGFs should not have any influence on the measured signal, even when IGFs$\to\infty$.

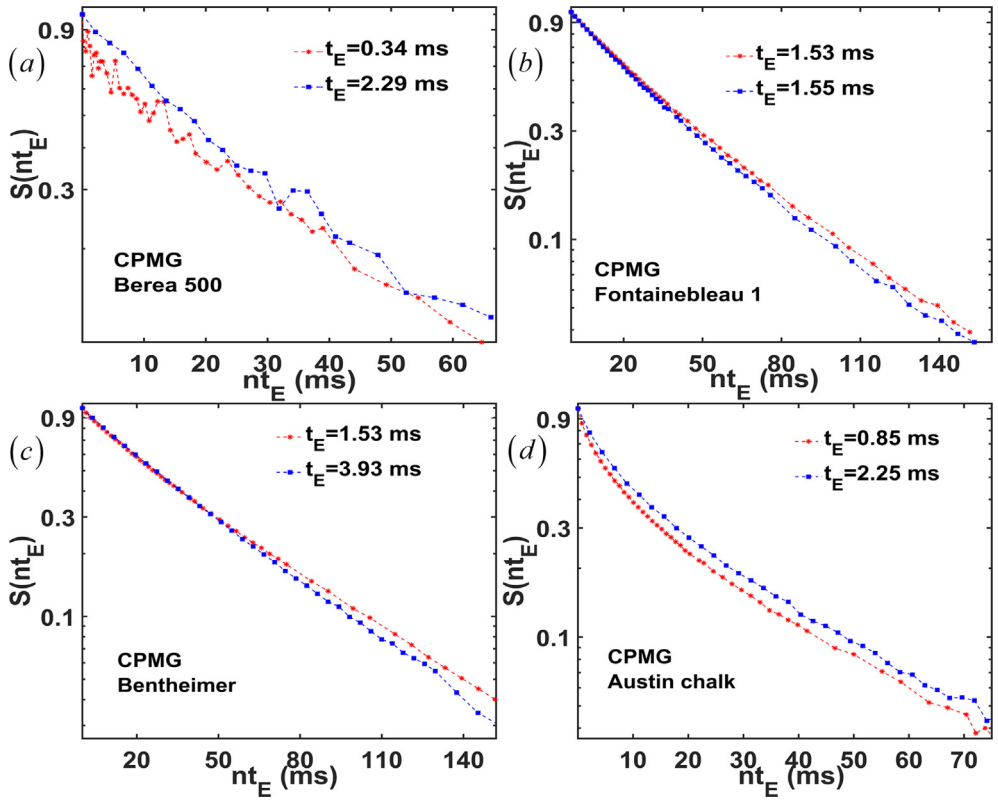

Fig. 5. Experimental CPMG $S(nt_E)$ signals as function of nt_E: (a) Berea 500, (b) Fontainebleau 1, (c) Bentheimer, (d) Austin for different values of rf-field, ν_{rf} and the delay time t_E: (a) ν_{rf} = 3.5 kHz and t_E = 0.34 ms – red line with stars, ν_{rf} = 0.5 kHz and t_E = 2.29 ms – blue line with squares; (b) ν_{rf} = 3 kHz and t_E = 1.53 ms – red line with stars, ν_{rf} = 4 kHz and t_E = 1.55 ms – blue line with squares; (c) ν_{rf} = 3 kHz and t_E = 1.53 ms – red line with stars, ν_{rf} = 3 kHz and t_E = 3.93 ms – blue line with squares; (d) ν_{rf} = 4 kHz and t_E = 0.85 ms – red line with stars, ν_{rf} = 4 kHz and t_E = 2.25 ms – blue line with squares. In all cases, $t_E = 2\tau + t_{180}$, where t_{180} is the length of 180°-pulse. The scale of axis x is linear and y is logarithmic. (For interpretation of the references to colour in this figure legend, the reader is referred to the web version of this article.)

If l_S value is very small, the ions will jump multiple times between walls with respect to the measured time, which will average out the influence of IGFs to some constant value. In the case of very large l_S, this influence is not averaged and it should be time dependent. Therefore, parameter B should have direct dependence on l_S.

Substituting Eq. (8) into Eq. (7), taking into account the second term only (the t_E^2 term), and comparing it with the known expression of the free diffusional regime without constants [27], one obtains

$$\frac{\left(D_0/l_s^2\right)^2}{T_D} t_E^2 \propto D_0 (\gamma g)^2 t_E^2 \tag{9}$$

where γ- is the gyromagnetic ratio and g is the internal magnetic field gradient (linear approximation). From this expression, one can obtain T_D. The value of T_D^{-1} is defined as:

$$T_D^{-1} \propto (\gamma g)^2 l_S^4 / D_0 \tag{10}$$

which defines the known motional averaging regime [27].

Therefore, free diffusional and motional averaging regimes are linked with each other and they are not independent as reported previously [15].

In the case when the brine is not diluted, in all Eqs. (8)–(10) the value of the pore size l_S is replaced on the mean free path, which determinates the average distance traveled by the sodium ion between collisions with other sodium ions.

The last statement can be validated experimentally. We performed additional experiments using 2 bulk. ^{7}LiCl solutions under 0.5 M and 15 M of concentrations were put in 5 mm glass tubes and SE experiments were performed (Fig. 9). ^{7}Li ions were chosen as detected spins due to their long relaxation times (in seconds).

Dependence of $T_{2,eff}^{-1}$ of lithium ions on t_E in the bulk samples can be described in the same way as in the case of sodium ions in the pores of the saturated rock samples (Eq. (6)).

The same behavior of $T_{2,\mathrm{eff}}^{-1}$ of lithium ions in the bulk samples can also be considered as an additional confirmation that SE experimental data are more reliable than CPMG. If we assume that the obtained SE T_2 values of sodium ions in all four rock samples are smaller than CPMG T_2 values due to the influence of the diffusion (and not due to another reason), we would not observe the same behavior of $T_{2,\mathrm{eff}}^{-1}$ for lithium and sodium ions.

Figs. 7 and 8, showed the influence of the diffusion in the presence of IGFs in the case of two of the sandstones, where during SE experiment free diffusional regime was transformed into motional averaging. For Berea 500 (Fig. 7a) the experimental and single decay signals fit well for all t_E. Therefore, for Berea 500 we could assume that the sodium ions are in motional averaging regime from the beginning of SE experiments. This assumption can be rebutted though, by performing ^{23}Na nutation experiments (sequence in Fig. 1a) for the four saturated rock samples, where the magnetization is measured as function of the flip angle of the excited pulse. Fig. 10 shows the results of ^{23}Na nutation experiments for the 4 saturated rock samples using different rf-fields, ν_{rf}.

Berea 500 has IGFs, which are detectible even at low magnetic field [49]. At 9.7 T, IGFs have strong influence, which is noticeable at 4 kHz of rf-field (Fig. 10a, thick black curve). Regardless on the value of rf-field the minimal negative signal is higher in absolute

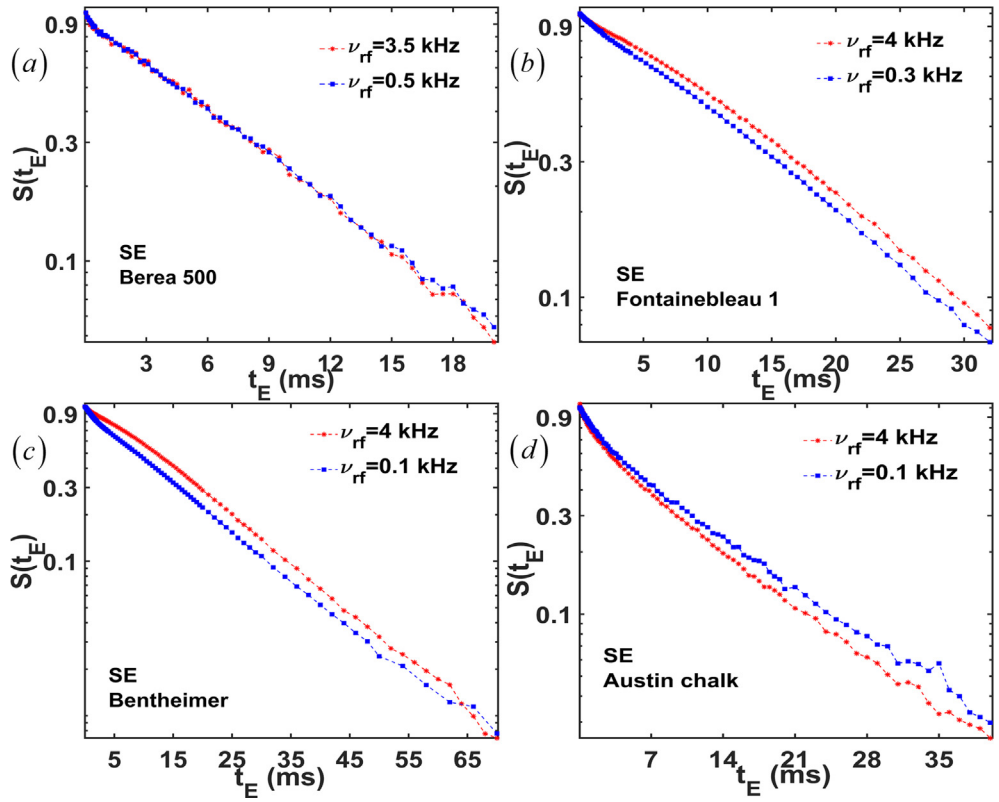

Fig. 6. Experimental SE $S(t_E)$ signals as function of t_E: (a) Berea 500, (b) Fontainebleau 1, (c) Bentheimer, (d) Austin for different values of rf-field, ν_{rf}: (a) ν_{rf} = 3.5 kHz – red line with stars, ν_{rf} = 0.5 kHz – blue line with squares; (b) ν_{rf} = 4 kHz – red line with stars, ν_{rf} = 0.3 kHz – blue line with squares; (c) ν_{rf} = 4 kHz – red line with stars, ν_{rf} = 0.1 kHz – blue line with squares; (d) ν_{rf} = 4 kHz – red line with stars, ν_{rf} = 0.1 kHz – blue line with squares. The scale of axis x is linear and y is logarithmic. (For interpretation of the references to colour in this figure legend, the reader is referred to the web version of this article.)

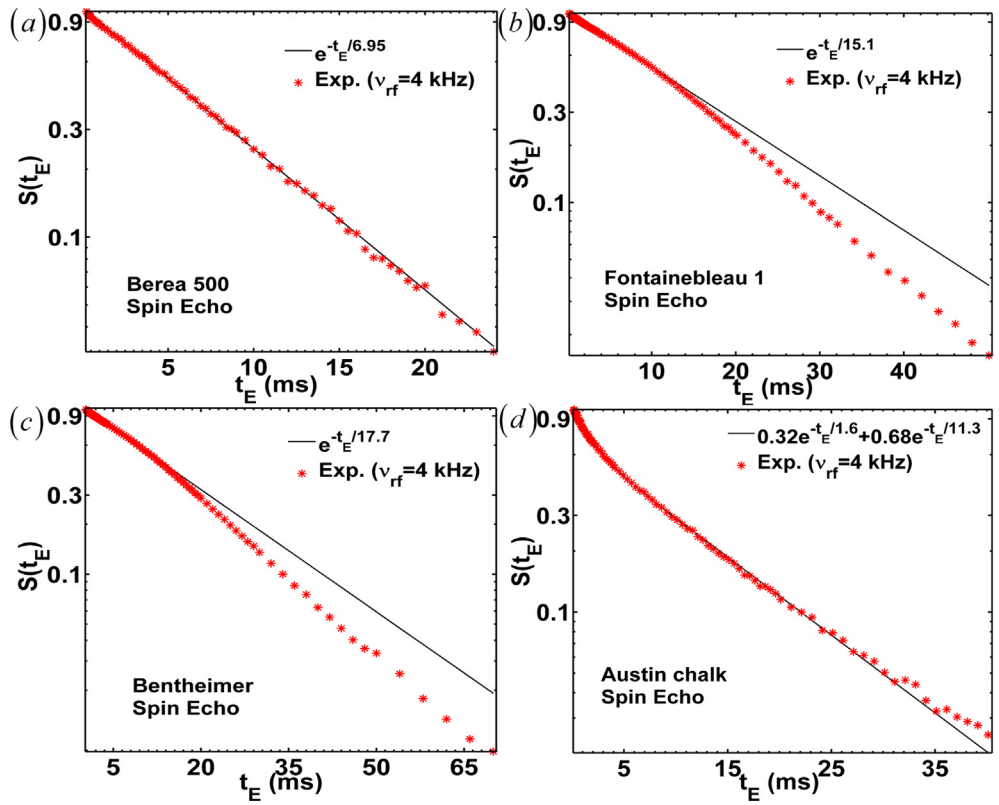

Fig. 7. Experimental (red) and the fitted (black) ^{23}Na SE data as a function of t_E: (a) Berea 500, T_2 = 6.95 ms; 1 (b) Fontainebleau 1, T_2 = 15.1 ms; (c) Bentheimer, T_2 = 17.7 ms (d) and Austin T_{2A} = 1.6 ms, T_{2B} = 11.3 ms. In all experiments ν_{rf} = 4 kHz. A mono-exponential fit was used in (a)–(c), and a bi-exponential fit for (d). The scale of the y-axis is logarithmic and x is linear. (For interpretation of the references to colour in this figure legend, the reader is referred to the web version of this article.)

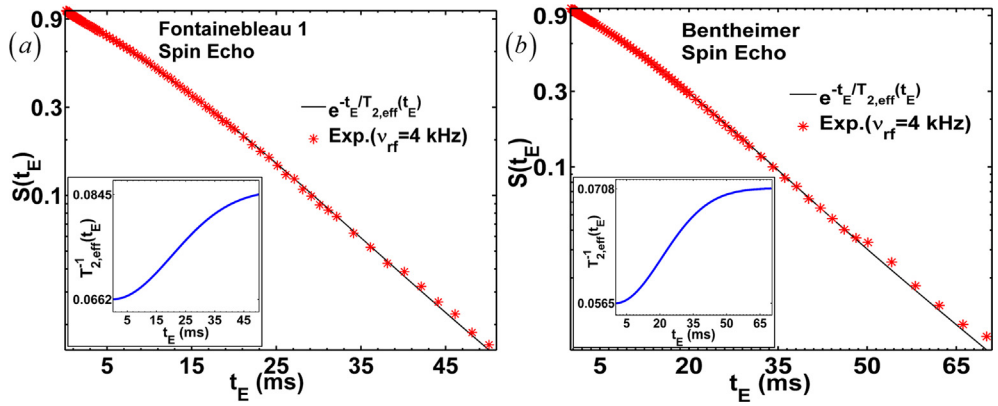

Fig. 8. The experimental (red, $\nu_{rf} = 4$kHz) and fitted (black) SE signals as a function of t_E for ^{23}Na in Fontainebleau 1 (a) and Bentheimer (b), where spin-spin relaxation includes the transition from the free diffusional regime to the motional averaging regime according to Eq. (6). Inserts show the functions describing the change of the effective T_2 rate. The fitted parameters become (a)$T_2 = 15.1$ ms, $T_D = 52.08$ ms, $B = 28.6$ ms; (b) $T_2 = 17.7$ ms, $T_D = 69.4$ ms, $B = 29.4$ ms. The scale of y-axis is logarithmic. (For interpretation of the references to colour in this figure legend, the reader is referred to the web version of this article.)

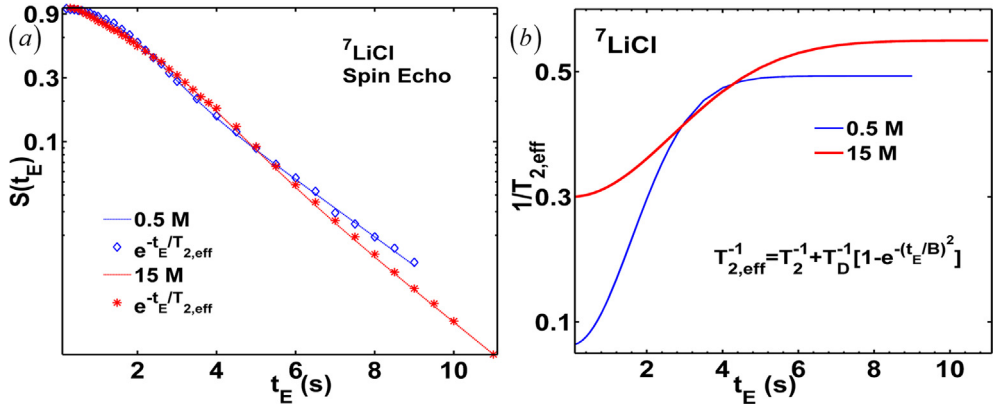

Fig. 9. (a) The experimental (markers, $\nu_{rf} = 4$kHz) and fitted (lines) SE signals as a function of t_E for ^{7}Li in 0.5 M (blue color) and 15 M (red color) of LiCl concentrations, where spin-spin relaxation includes the transition from the free diffusion regime to the motional averaging regime according to Eq. (6). The scale of y-axis is logarithmic and x-axis is linear. (b) Change of the effective T_2 rate in time in the case of 0.5 M (blue line) and 15 M (red line). The fitted parameters become: blue line - $T_2 = 15.87$ s, $T_D = 2.35$ s, $B = 2.24$ s; (b) $T_2 = 3.33$ s, $T_D = 4$ s, $B = 3.78$ s. (For interpretation of the references to colour in this figure legend, the reader is referred to the web version of this article.)

value with respect to the positive. The measured signal achieves the largest value under 0.5 kHz of rf-field with 227° of the flip angle.

It was previously shown that IGFs are relatively small at low magnetic fields for Fontainebleau 1 (Ref. [46]) and Bentheimer (Ref. [15]). The nutation curves in Fig. 10b, c are consistent with these findings – the minimal negative signal, which is higher in absolute value with respect to the positive signal, is detected under weak rf-field only (0.1 kHz, pink lines).

The last observation shows the similar behavior of the nutation curves for all three sandstones. Since for Fontainebleau 1 and Bentheimer the influence of the diffusion was observed after at least of 6 ms of echo time, the diffusion should not have an influence on sodium ions in Berea 500 during this period of time, too. Therefore, the diffusion does not have influence on the measured SE signals of Berea 500 in Fig. 7a.

The behavior of sodium ions in Austin chalk under weak rf-fields is opposite with respect to sandstones. For rf-fields like 0.5 kHz and 0.1 kHz the minimal negative signals in absolute values are smaller than the positive ones. This could be explained by strong spin-spin relaxation, or a residual quadrupolar distribution. The possibility of a residual quadrupolar distribution is considered latter in the next section.

To summarize this section, SE experiments show mono-exponential behavior of the measured signals in the case of the sandstones and multi-exponential behavior for Austin chalk. CPMG experiments show multi-exponential behavior of the measured signals for all the rock samples. CPMG experiments are found unreliable, because TQF experiments performed here (Fig. 3a–c) and previous knowledge of macroscopic mono-modal pore distributions prove that measured signals should have mono-exponential dependence.

For all the sandstones, the T_1 values are similar to that of NaCl solution, whereas the values of T_2 are significantly smaller (3–7.6 times).

Additionally, in the case of Fontainebleau 1 and Bentheimer, for $t_E \gtrsim 6$ ms, the diffusion in the presence of IGFs started to influence the experiments, which led to a decrease of T_2 in both the cases (Fig. 7b,c and Fig. 8). The quantitative influence of the diffusion on the total value of the relaxation time is described by Eq. (6). Sodium ions during the SE experiments are in free diffusion regime initially, which transforms to motional averaging regime after time $t_E > 1.7B$. This demonstrates that these regimes are linked and cannot be considered independently from each other. Such behavior is also detected in the bulk fluids like ^{7}LiCl solutions under different concentrations.

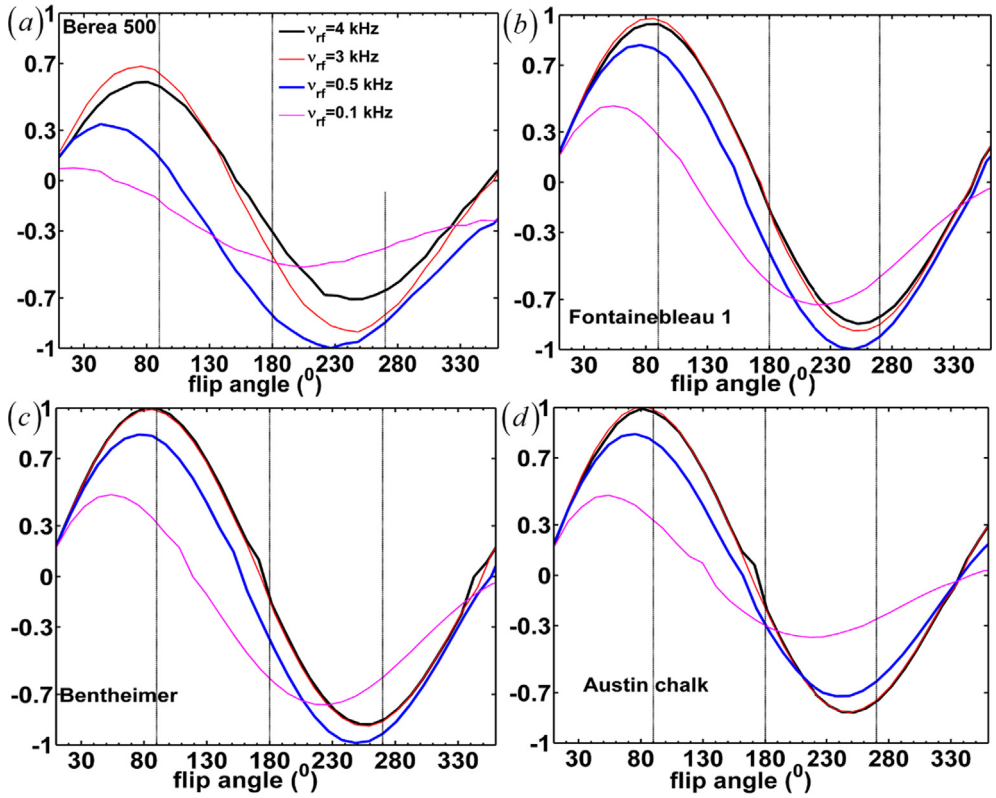

Fig. 10. Dependence of ^{23}Na signal in Berea 500 (a) Fontainebleau 1 (b), Bentheimer (c) and Austin (d) on the flip angle of Single Pulse (Fig. 1a) under different values of rf-field, ν_{rf}: ν_{rf} = 4 kHz – thick black line; ν_{rf} = 3 kHz – red line; ν_{rf} = 0.5 kHz – thick blue line and ν_{rf} = 0.1 kHz – pink line. All signals were normalized to the absolute maximum value of the signal for each sample. The maximum signal points are in Berea 500 for ν_{rf} = 0.5 kHz with flip angle 227°; in Fontainebleau 1 for ν_{rf} = 0.5 kHz with flip angle is 248°; in Bentheimer for ν_{rf} = 4 kHz with flip angle 85° and Austin for ν_{rf} = 4 kHz with flip angle 81°. The flip angles are based on the nominal flip angles at found at this power for a NaCl solution of concentration 0.4 M (5 mm quartz tube). All intensities were taken in absolute values. (For interpretation of the references to colour in this figure legend, the reader is referred to the web version of this article.)

The behavior of sodium ions inside porous media is definitely different from the behavior of protons in porous media or behavior of sodium ions in agarose gel. Decrease of T_2 and unchanged T_1 do not occur due to the influence of diffusion and not because ions are "outside the motional narrowing regime" (Ref. [21]).

This difference in the behavior is not easy to explain. The sodium ions are sensitive to the electric fields gradients, since the quadrupolar interaction is a consequence of the interplay between the quadrupolar moment of spins and the electric fields gradients. The electric fields gradients could also decelerate the motion of the ions to cause anisotropic motion and increase the rotational correlation time (τ_c), thereby affecting the relaxation rates further. In the case of Berea 500, strong paramagnetic impurities contribute to the electric fields also, thus leading to a larger decrease of T_2 in this rock as compared to other sandstones.

3.5. Austin chalk

Comparison between the simulated and the experimental data on Austin chalk (longitudinal TQF, QSP-SE) establishes the model of the distribution of sodium ions inside chalk pores.

Austin chalk displays a significant TQF signal (Fig. 3d). The origin of the signal is not self-evident. The case of a residual quadrupolar interaction needs to be considered too. In order to determine whether sodium ions have residual quadrupolar distribution or motion-induced bi-exponential relaxation, we compared the simulated and experimental transverse and longitudinal TQF signals. If the signal depends on bi-exponentially relaxing spins only, the obtained relaxation parameters in Fig. 11a (transverse TQF experiment) have to be the same as in Fig. 11b (longitudinal TQF experiment).

The obtained relaxation times in Fig. 11a and b have a large difference between them. For example, the short component of the T_{2s} is 0.53 ms in the case of Fig. 11a, whereas it equals to 7.75 ms in the case of Fig. 11b. Since the longitudinal TQF signal depends on the bi-exponential relaxation only, whereas the transverse TQF signal depends on the residual quadrupolar interaction it is reasonable to develop a model where sodium ions in Austin chalk has both a bi-exponential and a residual quadrupolar coupling pools of spins.

This is further investigated using a modified QSP-Spin Echo experiment (sequence in Fig. 1h), where the first 90°-pulse in the SE experiment was replaced by a QSP-block (sequence in Fig. 1g). The QSP-pulse is sensitive to the quadrupolar interaction (the sensitivity of QSP-pulse depends on the experimental parameters, ν_{rf} and κ, as was described in Ref. [44]). This pulse also excites the spins with different values of T_1 and T_2. However, the efficiency of the pulse is significantly smaller in the last case.

Therefore the QSP-SE experiment can be used as an additional tool for the investigation of the different types of spins. With the best-fit simulated data, we calculated the outcome of the QSP-SE signals and compared them with the experimental signal (Fig. 11c). The experimental QSP-SE signal (red stars) deviates from the simulated signals as a function of the delay time (the spectral densities were used from Fig. 11a and b in each case), which shows that sodium ions do not have bi-exponential relaxation and residual quadrupolar distribution at the same time.

Comparing the experimental and simulated data of four different experiments (longitudinal and transverse TQF, SE and QSP-SE), the relative population of sodium ions in Austin chalk was obtained. Table 4 shows the relative concentrations, relaxation times and the values of the quadrupolar distribution of the different types of sodium ions in Austin chalk.

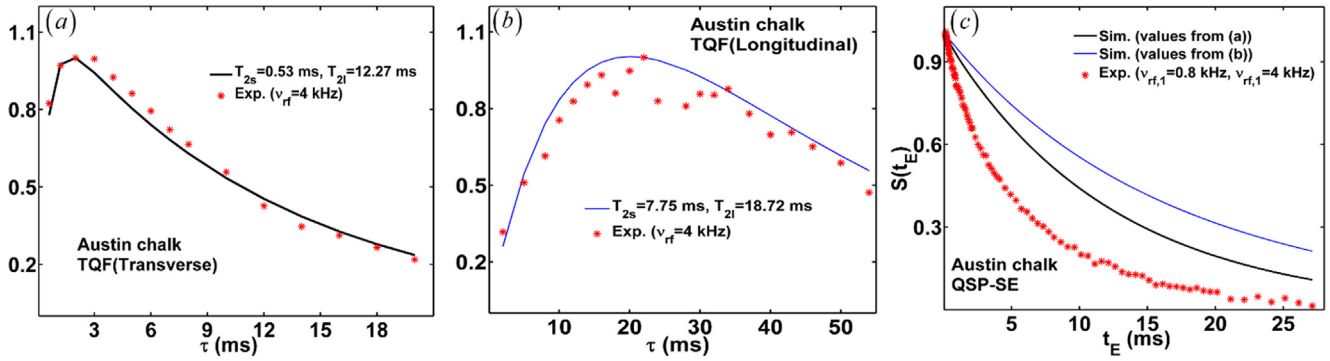

Fig. 11. (a) and (b) ^{23}Na experimental (red stars) and simulated optimal (blue and black lines) transverse (black curve) and longitudinal (blue curve) TQF curves as a function of τ: (a) The optimal values of spin-spin relaxation times are T_{2s} = 0.53 ms, T_{2l} = 12.27 ms and T_{1s} = 7.69 ms, T_{1l} = 29.94 ms ($J_0 = 1800$ Hz, $J_1 = 65$ Hz, $J_2 = 16.7$ Hz. J_0,J_1,J_2 are the spectral densities[35]); (b) The optimal values of spin–spin relaxation times are T_{2s} = 7.75 ms, T_{2l} = 18.72 ms and T_{1s} = 12.82 ms, T_{1l} = 34.72 ms ($J_0 = 90$ Hz, $J_1 = 39$ Hz, $J_2 = 14.4$ Hz). (c) ^{23}Na experimental (red diamonds) and simulated (blue and black lines) QSP-SE curves as a function of τ. The black curve was obtained with the values were found in (a) and the blue curve was obtained with the values found in (b). The rf-field (0.8 kHz) and the lengths of adjacent pulses (κ = 1.25 and t_p = 0.25 ms) were chosen such that the QSP signal had the maximal value. All simulations were performed using a set of tensor differential equations as described in Ref.[35]. (For interpretation of the references to colour in this figure legend, the reader is referred to the web version of this article.)

The ratios between the first, second, and third types are 0.12:0.39:0.49. The spins with concentrations of 49% and 39% have a quadrupolar distributions with single T_2 values of 5.75 ms and 0.75 ms, respectively. The probability of the quadrupolar distribution was modeled with the normalized Lorentzian function:

$$P(\nu_Q) = 2\pi^{-1}\gamma/\left[\gamma^2 + \nu_Q^2\right] \tag{11}$$

where $P(\nu_Q)$ is a probability to find a spin with the quadrupole frequency ν_Q. For 49% concentration, $\gamma = 0.21$ and the quadrupole frequency values span between $\nu_Q = [0:1.4]$ kHz, whereas for 39% concentration $\gamma = 0.3$ and the quadrupole frequency values span betwen $\nu_Q = [0:2]$ kHz.

The spins with 12% concentration has bi-exponential relaxation with values of spin-spin relaxation times T_{2s} = 4.48 ms and T_{2l} = 17.82 ms ($J_0 = 180$ Hz, $J_1 = 43$ Hz, $J_2 = 13.1$ Hz). The values of spin-lattice relaxation times are T_{1s} = 11.62 ms and T_{1l} = 38.2 ms.

Fig. 12 shows the experimental and the simulated transverse and longitudinal TQFs, SE and QSP-SE signals with these parameters.

There is a good agreement between the simulated and the experimental signals (Fig. 12). However, a deviation is observed in the SE experiment (Fig. 12c) after a delay time of ~22 ms. This deviation also can be explained with the influence of the IGFs in the presence of diffusion. After ~22 ms, only bi-exponentially relaxing spins contribute to the signal (because of the long part, T_{2l} = 17.82 ms), and therefore only they are subjected to the influence of the diffusion.

Fig. B1-3 in Appendix B provide further proof for the hypothesis of the distribution sodium ions in porous media of Austin chalk.

Fig. B1 shows that the location parameter in normalized Lorentzian function (Eqs. B(1) and B(2) in Appendix B), $\nu_{Q,mean}$, is zero and the probability of the quadrupolar distribution is described by Eq. (11). Fig. B2 shows QSP spectra at κ = 1.25 under different values of rf-field, in which background spectra become larger with increasing values of rf-field. The background spectrum is a sign of the presence of residual quadrupolar distribution.

Fig. B3 compares experimental and simulated QSP curves [44], which show a good agreement.

To summarize, this section shows the analysis of the experimental data of ^{23}Na in the pores of Austin chalk, obtained with different experiments. The model of the population distribution of sodium ions in the pores of Austin chalk was obtained by comparing the simulated and experimental signals in SE, TQFs and QSP experiments. The characteristics of the 3 populations are:

- 39% of the population have mono-exponential distribution with 0.75 ms T_2 and Lorentzian quadrupolar distribution with values between [0:2];
- 49% of the population have mono-exponential distribution with 5.75 ms T_2 and Lorentzian quadrupolar distribution with values between [0:1.4];
- 12% of the population have bi-exponential relaxation with T_{2s} = 4.48 ms, T_{2l} = 17.82 ms and zero averaged quadrupolar interaction.

The relative concentrations of 3 populations are not exact, since 8 variables were optimized to determine them (two relative populations, two mono-exponential values, two bi-exponential values, two quadrupolar distributions). However, we can say with certainty that spins with bi-exponential relaxation and residual quadrupolar distribution are different and the population of the first is significantly smaller with respect to the second.

Austin chalk has a dual microscopic pore system. 39% and 49% population of sodium ions are absorbed in the pores with smallest and largest sizes, respectively.

The third population of bi-exponentially relaxing spins arises from the exchange of spin ions between these different pores as well as between the walls and the bulk of the pores. This exchange leads to the dependence of this population on the influence of the diffusion in the presence of IGFs.

Table 4
The values of the relative concentrations, relaxation times and the values of the quadrupolar distribution sodium ions in Austin chalk based on assuming three types.

Group of spins	Relative concentration (%)	Type of the relaxation	T_2 (ms)	Type of the quadrupolar distribution	Width of the distribution (kHz)
1	12	bi-	4.48; 17.82	None	–
2	49	Mono-	5.75	Lorentzian	[0:1.4]
3	39	Mono-	0.75	Lorentzian	[0.:2]

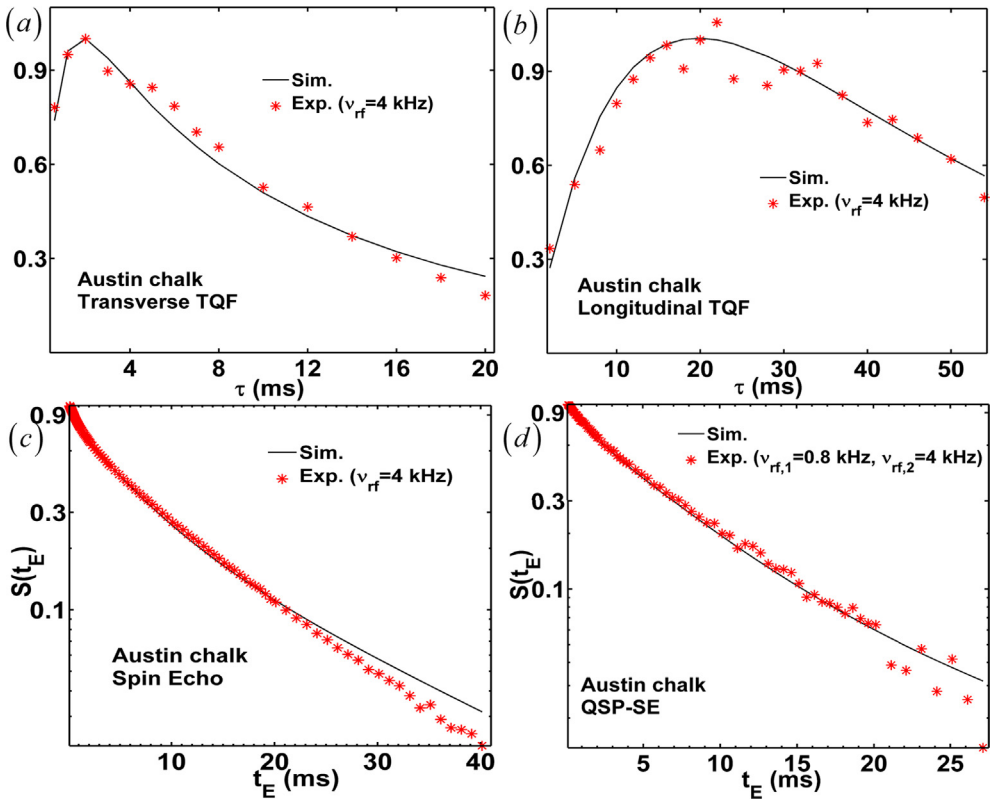

Fig. 12. (a) and (b) ^{23}Na experimental (red stars) and simulated (black line) transverse and longitudinal TQF curves as function of τ. $\nu_{rf} = 4$ kHz. (c) ^{23}Na experimental (red stars) and simulated SE curve (black line) as function of t_E. $\nu_{rf} = 4$ kHz. The scale of the y-axis is logarithmic. (d) ^{23}Na experimental (red stars) and simulated QSP-SE (black line) curves as function of τ. The scale of the y-axis is logarithmic. All simulated signals were calculated with the parameters are shown in Table 4. All simulations were performed using a set of tensor differential equations as described in Ref. [35]. (For interpretation of the references to colour in this figure legend, the reader is referred to the web version of this article.)

4. Conclusion

Here we reported the investigation of the unique properties of sodium ions in the pores of Berea 500, Fontainebleau 1, Bentheimer sandstones and Austin chalk under external magnetic field of 9.39 T.

SE experimental data were consistent with the previous observations – mono-exponential distributions for sandstones and multi-exponential for Austin chalk. CPMG experimental data demonstrated false multi-exponential distributions for sandstones.

Two models (Brownstein-Tarr model or "agarose gel model") could be used for characterization of the behavior of sodium ions inside porous media based on previous findings. The first model has been successfully used when protons are detected spins. The second model recently was applied in ^{23}Na 2D T_1-T_2 experiments, where mesoporous systems [20] and Stevns Klint chalk [21] porous media were investigated. However, our findings indicate that ions in general could not be accurately described by these two models.

Brownstein-Tarr model takes into account the influence of the diffusion in the presence of IGFs. However, it does not take into account the anisotropic motion which causes a decrease in T_2 and leaves T_1 unchanged; and the slow motion regime, which can cause bi-exponential relaxation and residual quadrupolar distribution in the same pore.

"Agarose gel model" considers the presence of bi-exponential relaxation only and therefore the influence of the diffusion, the anisotropic motion or residual quadrupolar distribution can be overlooked.

We showed with different NMR experiments that T_2 values of sodium ions inside all four saturated rock samples decreased due to the anisotropic motion. However, we did not provide any quantitative description of this phenomenon and further investigations are required. For the theoretical description, the interactions between the electric moments of sodium ions and the instantaneous electric moments linking to the porous media should be considered. In addition to anisotropic motion, for Fontainebleau 1, Bentheimer and Austin chalk we detected influence of the diffusion in the presence of IGFs. Moreover, we found the link between free diffusional and motional averaging regimes. We also demonstrated that the link between these two regimes could be detected in the bulk samples, e.g. LiCl solutions in 5 mm tubes. Since the quantitative link between these regimes were derived empirically, further investigation of this phenomenon is required.

In the case of Austin chalk, we obtained three different populations of sodium ions. Two of them had mono-exponential relaxation and Lorentzian residual quadrupolar distributions. The third small population had bi-exponential relaxation.

A new theoretical model is needed for the accurate interpretation of the unique behavior of spin ions.

Although pore size cannot be obtained directly from ^{23}Na relaxation experiments as in the case of ^{1}H experiments, different unique and important data can be obtained with these experiments.

We believe that the data and conclusions will be useful in future investigations where spins in ionic states are considered regardless of the size and nature of media.

Acknowledgments

The research was done in the group of Prof. Alexej Jerschow, New York University, USA and was supported with funding from the United States National Science Foundation, award No. CHE 1412064 for methodology development, and a grant from the American Chemical Society Petroleum Research Fund #57045-ND5 for work on rock samples.

I thank Prof. Yi-Qiao Song and Prof. Ravinath Kausik from Schlumberger-Doll Research Center, One Hampshire Street, Cambridge, MA 02139, USA for providing saturated rock samples. I am immensely grateful to Prof. Alexej Jerschow from New York University, Dr. Manali Gosh, Dr. Lisa Della Ripa and Prof. Taras Pogorelov from University of Illinois at Urbana-Champaign for helping with edition of the manuscript.

Appendix A

Inverse Laplace transforms of SE and CPMG experiments

Fig. A1 shows T_2 distribution from CPMG data. In all four cases, the distributions are multi-exponential (Fig. A1b–e). For comparison, T_2 probability distribution of sodium ions in NaCl solution (0.135 M) is shown (Fig. A1a).

Fig. A2 shows T_2 distribution from SE data. The distributions for 3 sandstones are mono-exponential (Fig. A2b–d) and for Austin

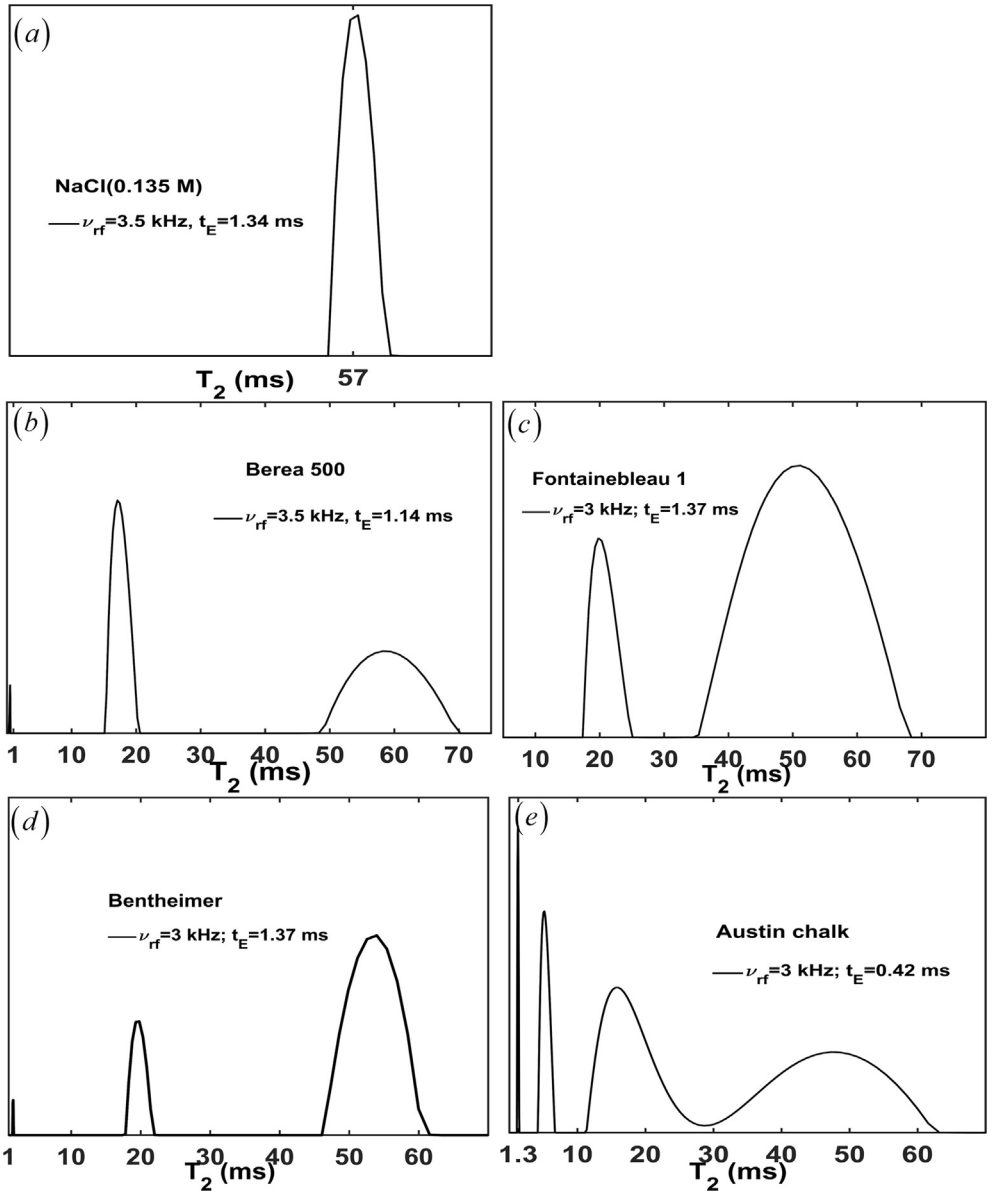

Fig. A1. Probability distribution of T_2 of ^{23}Na CPMG experiments in NaCl (a), Berea 500 (b), Fontainebleau 1 (c), Bentheimer (d) sandstones and Austin chalk (e). The scale of x-axis and y-axis are linear.

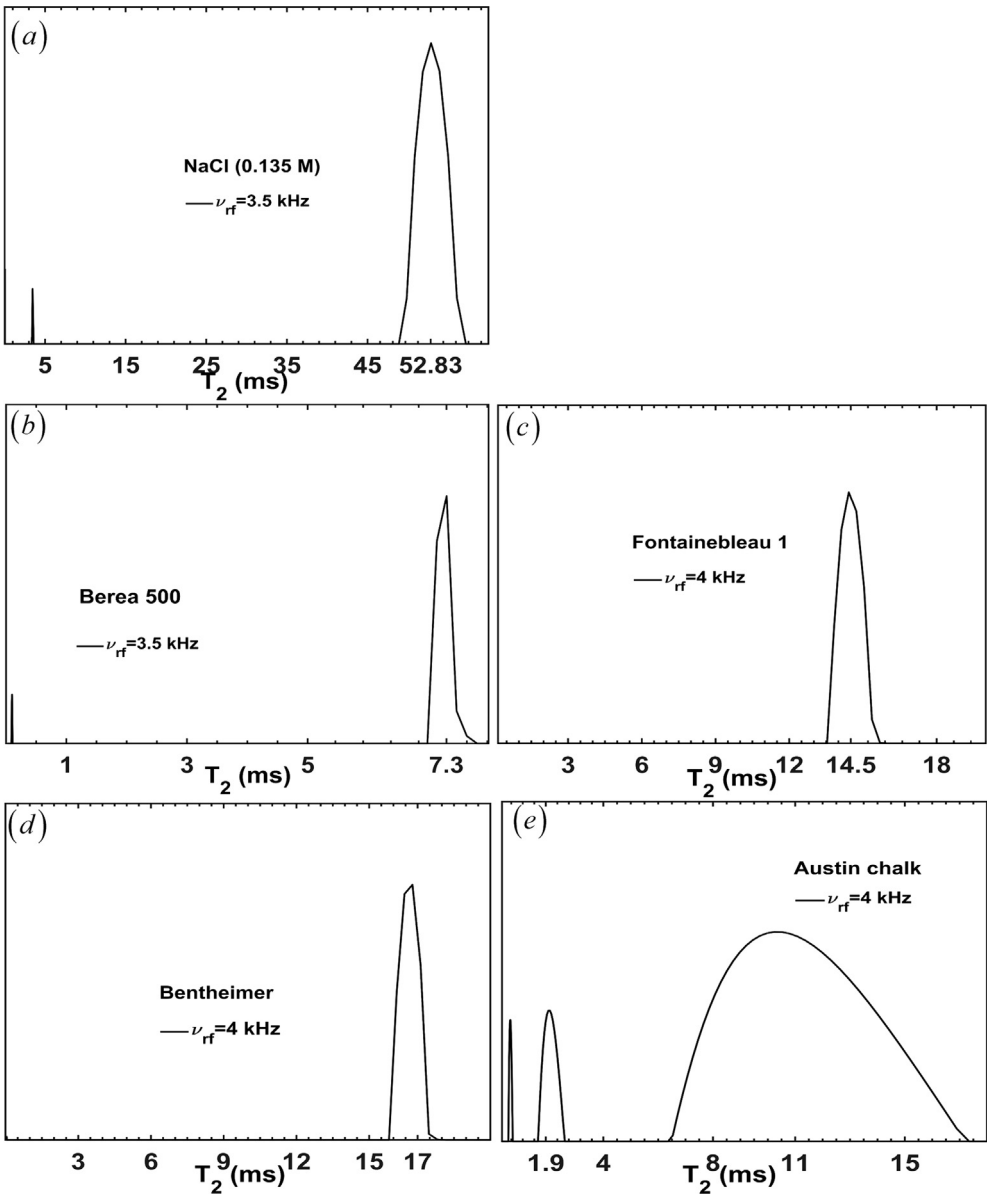

Fig. A2. Probability distribution of T_2 of ^{23}Na SE experiments in NaCl (a), Berea 500 (b), Fontainebleau 1 (c), Bentheimer (d) sandstones and Austin chalk (e). The scale of x-axis and y-axis are linear.

chalk is multi-exponential (Fig. A2e). For comparison, T_2 probability distribution of sodium ions in NaCl solution (0.135 M) is shown (Fig. A2a).

Appendix B

QSP experiments

We assume here that the quadrupolar distribution of sodium ions in the pores of Austin chalk can be considered as Lorentzian:

$$P(\nu_Q) = 2\pi^{-1}\gamma/\left[\gamma^2 + (\nu_Q - \nu_{Q,mean})^2\right] \quad \text{(B1)}$$

where $\nu_{Q,mean}$ is the mean quadrupole frequency (the localization parameter), and $\nu_Q \geq \nu_{Q,mean}$.

Fig. B1a and b show the simulated QSP curves when $\nu_{Q,mean} = 0$ (a) and when $\nu_{Q,mean} = 0.2$kHz (b). Fig. B1c shows experimental QSP data of sodium ions in Austin chalk.

When $\nu_{Q,mean} \neq 0$ (Fig. B1b), the behavior of the simulated QSP curves depends on the values of the rf-field significantly, whereas for $\nu_{Q,mean} = 0$, the reverse is true. The trend for $\nu_{Q,mean} = 0$ is also observed in the QSP experiments (Fig. B1c). Therefore, we conclude that sodium ions in Austin chalk can have a quadrupolar distribution with $\nu_{Q,mean} = 0$ and Eq. (B1) can be written as:

$$P(\nu_Q) = 2\pi^{-1}\gamma/\left[\gamma^2 + \nu_Q^2\right] \quad \text{(B2)}$$

Fig. B2 shows QSP spectra under different values of ν_{rf} and $\kappa = 1.25$.

In all cases of Fig. B2, we observe that the width of the background spectrum increases until $\nu_{rf} = 0.8$ kHz (the QSP signal has a maximal intensity of 5.3% with respect to the hard 90°-pulse signal). Beyond this power, the width no longer changes with increasing rf-field. This proves that some parts of the sodium ions in Austin chalk have a residual quadrupolar distribution.

Fig. B3 compares the experimental (red stars) and simulated (black lines) QSP curves of sodium ions in Austin chalk, where

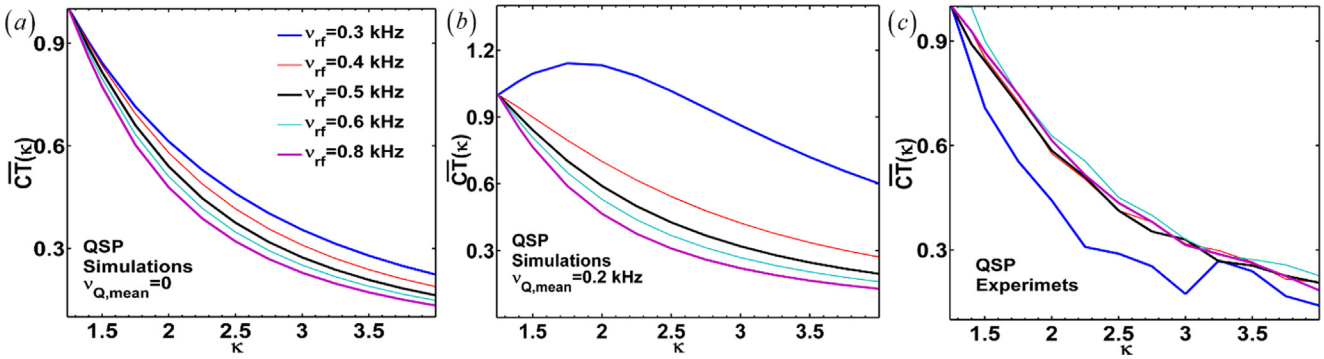

Fig. B1. (a) and (b) Simulated QSP curves under different values of ν_{rf}, when $\nu_{Q,mean} = 0$ (a) and $\nu_{Q,mean} = 0.2$ kHz. In two cases $\gamma = 0.15$. (c) ^{23}Na QSP curves in Austin chalk under different values of ν_{rf}. In all cases, ν_{rf} (kHz) = 0.3 (thick blue line), 0.4 (red line), 0.5 (thick black line), 0.6 (cyan line), 0.8 (thick pink line). (For interpretation of the references to colour in this figure legend, the reader is referred to the web version of this article.)

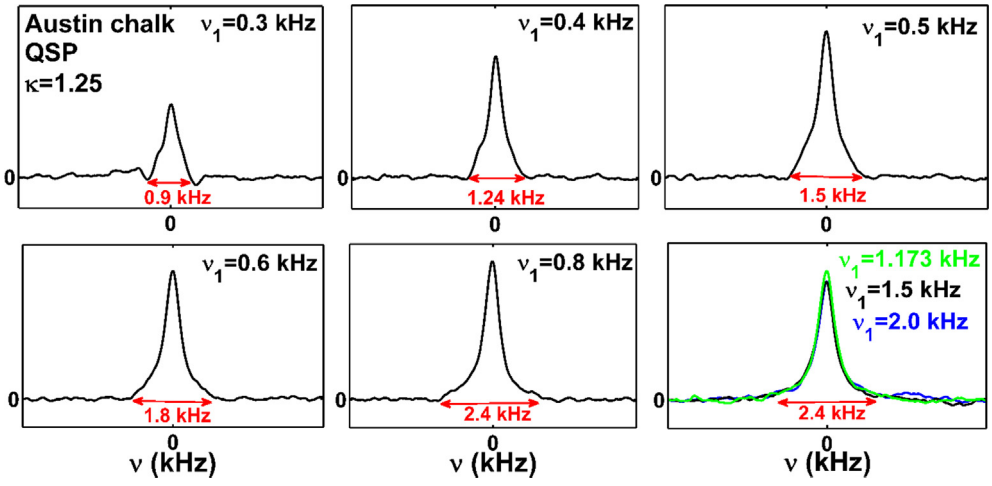

Fig. B2. ^{23}Na QSP spectra in Austin chalk for different values of rf-freld: ν_{rf} = 0.3, 0.4, 0.5, 0.6, 0.8, 1.173, 1.5, 2 (kHz). In all cases, $\kappa = 1.25$.

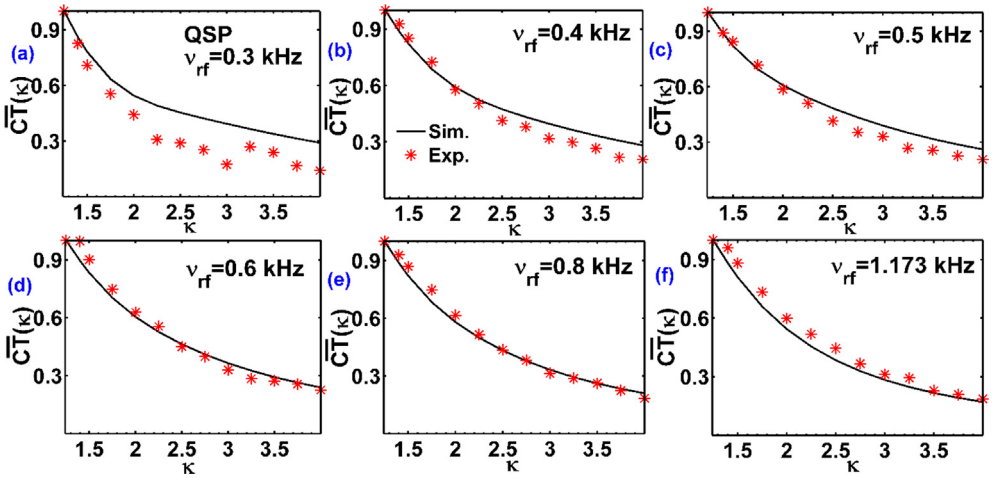

Fig. B3. The comparison of the experimental (red stars) and simulated (black lines) QSP curves for different values of the rf-field: ν_{rf} (kHz) = 0.3 (a), 0.4 (b), 0.5 (c), 0.6 (d), 0.8 (e) and 1.173 (f). (For interpretation of the references to colour in this figure legend, the reader is referred to the web version of this article.)

simulations were performed with the parameters from Table 4 in the main article. The simulated QSP curves are in good agreement with the experimental data points for different values of rf-field. In Fig. B3a, the simulated QSP curve has a significant deviation from the experimental data with respect to the other cases. This deviation can be explained with the influence of rf inhomogeneity and IGFs during weak pulses (0.3 kHz). Nevertheless, the dependence of QSP on κ is similar in both simulated and experimental data.

References

[1] L. Petrakis, E. Edelheit, The utilization of nuclear magnetic resonance spectroscopy for petroleum, coal, oil shale, petrochemicals, and polymers. Phenomenology, paradigms of applications, and instrumentation, Appl. Spectrosc. Rev. 15 (1979) 195–260.
[2] H.A. Resing, NMR relaxation of adsorbed molecules with emphasis on adsorbed water, Adv. Mol. Relax. Process. 3 (1972) 199–226.
[3] J.D. Loren, J.D. Robinson, Relations between pore size fluid and matrix properties, and NML measurements, Soc. Pet. Eng. J. 10 (1970) 268–278.
[4] R.L. Kleinberg, S.A. Farooqui, M.A. Horsfield, T1/T2 ratio and frequency dependence of NMR relaxation in porous sedimentary rocks, J. Colloid Interface Sci. 158 (1993) 195–198.
[5] H. Rueslåtten, T. Eidesmo, K.A. Lehne, O.M. Relling, The use of NMR spectroscopy to validate NMR logs from deeply buried reservoir sandstones, J. Pet. Sci. Eng. 33–43 (1998), https://doi.org/10.1016/S0920-4105(97)00033-8.
[6] Y. Tanino, M.J. Blunt, Capillary trapping in sandstones and carbonates: dependence on pore structure, Water Resour. Res. 48 (2012) 1–13.
[7] P.E. Øren, S. Bakke, Reconstruction of Berea sandstone and pore-scale modelling of wettability effects, J. Pet. Sci. Eng. 39 (2003) 177–199.
[8] C. Straley, G. Leu, Low-Field NMR Profiles for Verification of Oil and Water Saturations in Cores, 2006.
[9] R.M. Henkelman, G.J. Stanisz, J.K. Kim, M.J. Bronskill, Anisotropy of NMR properties of tissues, Magn. Reson. Med. 32 (1994) 592–601.
[10] P. Porion et al., A NMR investigation of adsorption/desorption hysteresis in porous silica gels, Magn. Reson. Imag. 16 (1998) 679–682.
[11] E. Grunewald, R. Knight, Pore coupling in heterogeneous media, Geophysics 74 (2009) 215–221.
[12] J. Mitchell, E.J. Fordham, Contributed review: Nuclear magnetic resonance core analysis at 0.3 T, Rev. Sci. Instrum. 85 (2014).
[13] E. Grunewald, R. Knight, The effect of pore size and magnetic susceptibility on the surface NMR relaxation parameter T*2, Surf. Geophys. 9 (2011) 169–178.
[14] R. Freedman et al., Wettability, saturation, and viscosity from NMR measurements, SPE J. 8 (2003) 317–327.
[15] J. Mitchell, T.C. Chandrasekera, M.L. Johns, L.F. Gladden, E.J. Fordham, Nuclear magnetic resonance relaxation and diffusion in the presence of internal gradients: the effect of magnetic field strength, Phys. Rev. E - Stat. Nonlinear Soft Matter Phys. 81 (2010) 1–19.
[16] D. Yang, R. Kausik, 23Na and 1H NMR relaxometry of shale at high magnetic field, Energy Fuels 30 (2016) 4509–4519.
[17] L.R. Stingaciu et al., Characterization of unsaturated porous media by high-field and low-field NMR relaxometry, Water Resour. Res. 45 (2009).
[18] P.N. Tutunjian, H.J. Vinegar, J.A.F. Shell, D. Company, Nuclear magnetic resonance imaging of sodium-23 in cores, Log Anal. (1988).
[19] L.A. Rijniers, P.C.M.M. Magusin, H.P. Huinink, L. Pel, K. Kopinga, Sodium NMR relaxation in porous materials, J. Magn. Reson. 167 (2004) 25–30.
[20] R. Kausik, K. Fellah, D.M. Yang, Sodium NMR relaxation in mesoporous systems, Microporous Mesoporous Mater. 269 (2018) 134–137.
[21] J. Mitchell, E.J. Fordham, Sodium-23 NMR in porous media, Microporous Mesoporous Mater. 269 (2018) 109–112.
[22] J. Kärger, R. Valiullin, Diffusion in porous media, Encycl. Magn. Reson. 1–14 (2011), https://doi.org/10.1002/9780470034590.emrstm0121.pub2.
[23] G.Q. Zhang, G.J. Hirasaki, W.V. House, Internal field gradients in porous media, Petrophysics 44 (2003) 422–434.
[24] M.H. Cohen, K.S. Mendelson, Nuclear magnetic relaxation and the internal geometry of sedimentary rocks, J. Appl. Phys. 53 (1982) 1127–1135.
[25] K.E. Washburn, Relaxation mechanisms and shales, Concepts Magn. Reson. Part Bridg. Educ. Res. 43A (2014) 57–78.
[26] R.L. Kleinberg, M.A. Horsfield, Transverse relaxation processes in porous sedimentary rock, J. Magn. Reson. 1969 (88) (1990) 9–19.
[27] M.D. Hürlimann, Effective gradients in porous media due to susceptibility differences, J. Magn. Reson. San Diego Calif. 1997 (131) (1998) 232–240.
[28] R.M.E. Valckenborg, H.P. Huinink, J.J.V.D. Sande, K. Kopinga, Random-walk simulations of NMR dephasing effects due to uniform magnetic-field gradients in a pore, Phys. Rev. E - Stat. Nonlinear Soft Matter Phys. 65 (2002) 1–8.
[29] J. Mitchell et al., Relaxation analysis of porous media at high magnetic field strengths: the influence of internal gradients, AIP Conf. Proc. 1330 (2011) 35–38.
[30] H.J. Cho, E.E. Sigmund, Y. Song, Magnetic resonance characterization of porous media using diffusion through internal magnetic fields, Materials 5 (2012) 590–616.
[31] M.D. Hürlimann, K.G. Helmer, T.M. Deswiet, P.N. Sen, Spin echoes in a constant gradient and in the presence of simple restriction, J. Magn. Reson. Ser. A 113 (1995) 260–264.
[32] R.V. Pound, Nuclear electric quadrupole interactions in crystals, Phys. Rev. 79 (1950) 685–702.
[33] H.J. Berendsen, H.T. Edzes, The observation and general interpretation of sodium magnetic resonance in biological material, Ann. N.Y. Acad. Sci. 204 (1973) 459–485.
[34] D.E. Woessner, NMR relaxation of spin-3/2 nuclei: Effects of structure, order, and dynamics in aqueous heterogeneous systems, Concepts Magn. Reson. 13 (2001) 294–325.
[35] J.R.C. Van Der Maarel, Thermal relaxation and coherence dynamics of spin 3/2. I. Static and fluctuating quadrupolar interactions in the multipole basis, Concepts Magn. Reson. Part Bridg. Educ. Res. 19 (2003) 97–116.
[36] G. Madelin, J. Lee, R.R. Regatte, A. Jerschow, Sodium MRI: methods and applications, Prog. Nucl. Magn. Reson. Spectrosc. 79 (2014) 14–47.
[37] W.D. Rooney, J. Springer, A comprehensive approach to the analysis and interpretation of the resonances of spins 3/2 from-living systems, NMR Biomed. 4 (1991) 209–226.
[38] U. Eliav, G. Navon, Sodium NMR/MRI for anisotropic systems, NMR Biomed. (2015).
[39] K.R. Brownstein, C.E. Tarr, Importance of classical diffusion in NMR studies of water in biological cells, Phys. Rev. A 19 (1979) 2446–2453.
[40] G.S. Payne, P. Styles, Multiple-quantum-filtered 23Na NMR spectroscopy in model systems, J. Magn. Reson. 1969 (95) (1991) 253–266.
[41] E.L. Hahn, Spin echoes, Phys. Rev. 80 (1950) 580–594.
[42] H. Carr, E. Purcell, Effects of diffusion on free precession in nuclear magnetic resonance experiments, Phys. Rev. 94 (1954) 630–638.
[43] R.L. Vold, J.S. Waugh, M.P. Klein, D.E. Phelps, Measurement of spin relaxation in complex systems, J. Chem. Phys. 48 (1968) 3831–3832.
[44] E. Nimerovsky, A. Jerschow, Quadrupole sensitive pulse for signal filtering, J. Magn. Reson. 265 (2016) 153–163.
[45] P.D. Teal, C. Eccles, Adaptive truncation of matrix decompositions and efficient estimation of NMR relaxation distributions, Inverse Probl. 31 (2015) 045010.
[46] P.E. Øren, F. Antonsen, H.G. Rueslåtten, S. Bakke, Numerical simulations of NMR responses for improved interpretations of NMR measurements in reservoir rocks, Proc. SPE Annu. Tech. Conf. Exhib. 1–10 (2002), https://doi.org/10.2523/77398-MS.
[47] R. Oughanem et al., Pore-scale to core-scale study of capillary desaturation curves using multi-scale 3D imaging, Int. Symp. Soc. Core Anal. 1–13 (2013).
[48] K. Pearson, Geologic Models and Evaluation of Undiscovered Conventional and Continuous Oil and Gas Resources — Upper Cretaceous Austin Chalk, U.S. Gulf Coast Scientific Investigations Report 2012 – 5159. 26, 2012.
[49] M.D. Hürlimann, L. Venkataramanan, Quantitative measurement of two-dimensional distribution functions of diffusion and relaxation in grossly inhomogeneous fields, J. Magn. Reson. San Diego Calif. 1997 (157) (2002) 31–42.
[50] C. Tanase, F.E. Boada, Triple-quantum-filtered imaging of sodium in presence of B(0) inhomogeneities, J. Magn. Reson. San Diego Calif. 1997 (174) (2005) 270–278.